

# Applicability of *IsoFilter*<sup>TM</sup> Selectivity to Antenna Diagnostics

Doren W. Hess\* & Scott McBride<sup>+</sup>

MI Technologies  
1125 Satellite Blvd, Suite 100., Suwanee, GA 30024 USA  
(dhess\*, smcbride<sup>+</sup>)@mi-technologies.com

**Abstract**— We have devised a method for identifying the locations and strengths of an antenna's radiation sources that is an alternative to conventional back-projection. This alternative method utilizes the antenna's measured far-field radiation pattern and successive spherical modal analyses to ascertain the relative strength of the antenna's sources, as a function of position, that give rise to the farfield.

## I. INTRODUCTION

The early work with the *IsoFilter*<sup>TM</sup> technique demonstrated that the radiation emanating from the aperture of a horn, located several wavelengths above a ground plane, could be separated from the radiation due to the sidelobe and backlobe illumination of the ground plane itself. The success of this demonstration encouraged us to pursue further the question of how well the *IsoFilter*<sup>TM</sup> technique worked to suppress other types of secondary signals – such as signals coming from other elements of an array antenna or another individual first-order primary radiator nearby.

In the process of evaluating the goodness of the secondary signal suppression we have devised a method [1] for identifying the locations and strengths of an antenna's radiation sources that is an alternative to conventional back-projection. The alternative method utilizes the antenna's far-field measured radiation pattern and successive spherical modal analyses to ascertain the relative strength of the antenna's sources that give rise to its far field. We believe that this alternative technique has applicability to the general problem of antenna diagnostics.

The method employs repetitive application of the phase-multiplication operation upon the pattern to generate a translation of the origin -- i.e. the phase-multiplied pattern having a new spherical coordinate origin. A spherical modal analysis yielding the strength of the lowest order dipole gives the strength of the antenna sources corresponding to that location. As the multiplication process with various translations is repeated and then analyzed, a mapping of the strengths of the antenna sources in the vicinity of the antenna is produced. In this paper we recount the results so far obtained and compare them to conventional imaging by plane-wave back-projection.

## II. QUANTIFYING THE ISOFILTER<sup>TM</sup> REJECTION

The goal of the *IsoFilter*<sup>TM</sup> is to reject the influence of radiating sources that exist outside the sphere containing the sources of interest. This goal is analogous to a low-pass filter's goal of rejecting frequencies above the filter's cutoff. Just as there is no such thing as the frequently called-for 'ideal low-pass filter', we should expect some residual interference that the *IsoFilter*<sup>TM</sup> does not reject.

In this paper we take two approaches to evaluating the *IsoFilter*<sup>TM</sup> rejection. The first approach is to start with a small antenna at the origin, then *IsoFilter*<sup>TM</sup> to spheres whose centers move along the coordinate axes. Once the filtering sphere no longer contains any radiating sources, any reported signal represents interference that would add to the desired signal from an antenna located inside the filtering sphere. This approach was taken using both measured and synthesized data. The second approach is to synthesize a sparse array, then see how well we can reconstruct the pattern of the center element.

We first demonstrate an empirical procedure by which we may quantify the degree of rejection offered by the *IsoFilter*<sup>TM</sup> method. Recall first the configuration of the spherical near-field range on which the measurements for demonstrating *IsoFilter*<sup>TM</sup> were taken. It consisted of a roll-over-azimuth positioner with a fixed probe antenna. The pyramidal horn antenna was mounted above a ground plane, offset by 6 in along the roll axis. The roll and azimuth axes crossed at a point that lay precisely upon the ground plane surface. Please see Figure 1 for a photograph of the setup, where the horn is centered above the ground plane on the roll axis. The ground plane was covered by a panel of absorber to form a measurement configuration we refer to as the "bare horn" configuration, shown in Figure 2. It was demonstrated earlier that the *IsoFilter*<sup>TM</sup> technique provided a pattern measurement result of the horn above the ground plane that agreed well with the measured pattern of the bare horn. We use that bare horn pattern data taken earlier as the basis for ascertaining a quantitative measure of the degree of rejection provided by *IsoFilter*<sup>TM</sup>.

To give a feel for the pattern of the bare horn a spherical isometric plot showing the measured forward hemisphere is provided in Figure 3.

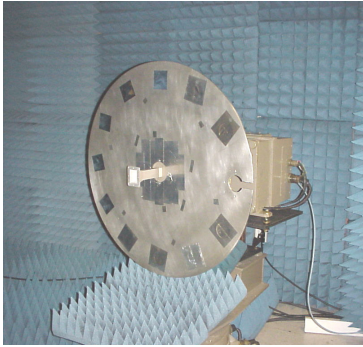


Figure 1 - Photograph of Spherical Near-Field Positioner for Measurement of an Antenna Above a Ground Plane

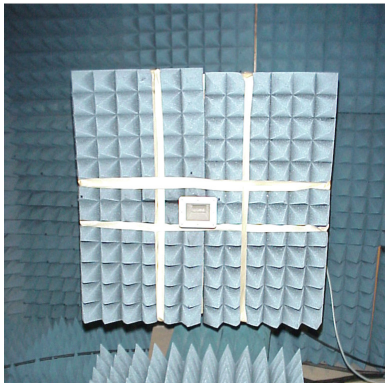


Figure 2 - Photograph of the Configuration for Measurements of the Bare Pyramidal Horn Antenna

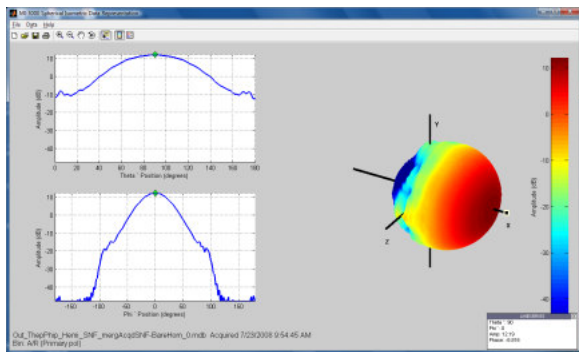


Figure 3 Spherical Isometric Plot of Forward Hemisphere of Bare Pyramidal Horn

After translating to the center of the aperture of the horn, the spherical modal distribution occupies modal bins that extend only up to modal order  $n = 5$ , as shown in the tabulation exhibited in Figure 5 below.

Figure 5 below illustrates the process we used to determine the *IsoFilter*<sup>TM</sup> rejection for the measured horn data. The *IsoFilter*<sup>TM</sup> sphere was translated along the X axis from 0" to 18" in 0.1" steps.

Amount of POWER (in watt) for each POLAR mode		
N	POWER	Accumulated POWER
1	2.3479439E-01	2.3479439E-01
2	1.6614209E-01	4.0093648E-01
3	7.2364792E-02	4.7330129E-01
4	1.9712446E-02	4.9301374E-01
5	4.5521087E-03	4.9756584E-01

Figure 4 - Summary Tabulation of Accumulated Power in Spherical Modes for Bare Horn with Origin Centered at Aperture

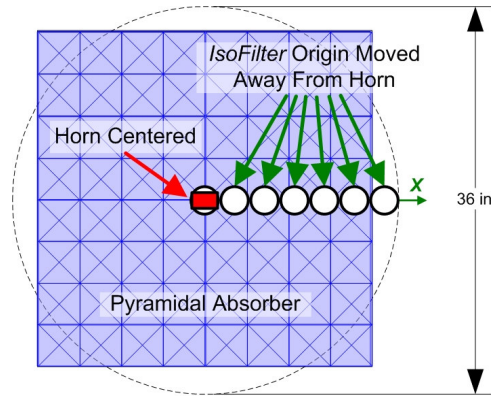


Figure 5 – Locus of Points Where *IsoFilter*<sup>TM</sup> Rejection Was Evaluated

For translations large enough that the horn is no longer contained in the *IsoFilter*<sup>TM</sup> sphere, the desired transform output should contain zero power. Any power reported in those outer spheres therefore represents imperfect *IsoFilter*<sup>TM</sup> rejection. If there were an AUT contained in a particular *IsoFilter*<sup>TM</sup> sphere, then the signal returned by this procedure represents a stray signal that would be added to the AUT signal we would be trying to isolate.

The sequence of translations corresponded to points along the x-axis of the measurement coordinate system, which lies in the H-plane of the horn. The data were measured at 8.0 GHz, so the 0-18" translations corresponded to approximately 0-12.2 wavelengths.

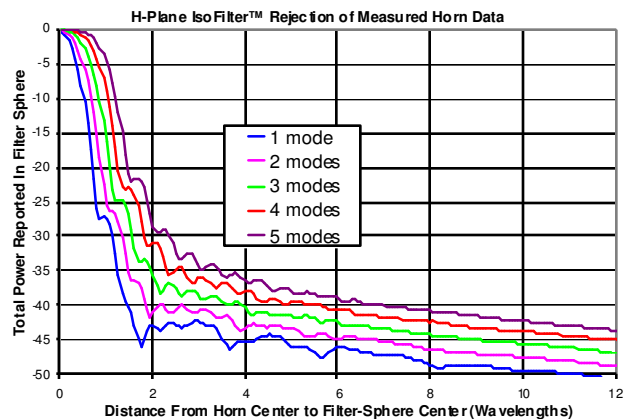


Figure 6 - *IsoFilter*<sup>TM</sup> Rejection of Measured Horn Along x-Axis. Plot of Normalized Total Power versus Radial Distance of Filter Sphere from Center

The *IsoFilter*<sup>TM</sup> technique was applied over and over in steps of 0.1", and the level of the accumulated power in spherical modes corresponding to modal orders 1 through 5 was plotted as a function of translation distance. The result is shown in Figure 6.

Figure 6 above demonstrates that *IsoFilter*<sup>TM</sup> can provide good rejection (>35 dB) against other pattern contributors provided that the other contributors are at least 4 wavelengths distance from the radiator of interest. Note that the horn used has a physical width of about 2λ at this frequency, and that there is significant rejection (>25 dB) as soon as the horn passes outside of the *IsoFilter*<sup>TM</sup> sphere (at the X-axis value of 2 in Figure 6). The use of five modes implies that the hypothetical AUT we are trying to isolate from the one horn measured can also be represented by five modes.

To investigate further the degree of rejection that *IsoFilter*<sup>TM</sup> might provide we next proceeded to investigate its performance using a simulated antenna.

### III. QUANTIFYING THE ISOFILTER<sup>TM</sup> REJECTION WITH A SIMULATED SMALL ANTENNA

The second step in our investigation was to compute the rejection of *IsoFilter*<sup>TM</sup> for an antenna smaller than the pyramidal horn that would be formed by modeling. This was done in the interest of learning the applicability of *IsoFilter*<sup>TM</sup> to phased-array diagnostics. We chose one of the simplest small antennas we knew of to investigate -- namely a pair of x-polarized dipole elements separated by half a wavelength in z and formed into a little endfire array with a backlobe null at 180 degrees. With the coordinate origin half way between the elements, the spherical modal power distribution is shown in Figure 7. From this tabulation it is clear that no more than three modal orders are needed to represent the element pattern. The resulting rejection curve is shown in Figure 9.

Amount of POWER (in watt) for each POLAR mode		
N	POWER	Accumulated POWER
1	1.0364673E+06	1.0364673E+06
2	9.7246445E+04	1.1337138E+06
3	3.0902712E+03	1.1368040E+06
4	4.7776115E+01	1.1368518E+06
5	4.3199185E-01	1.1368521E+06
6	2.5503063E-03	1.1368521E+06
7	1.0587692E-05	1.1368521E+06
8	4.2100336E-08	1.1368521E+06
9	4.8599152E-10	1.1368521E+06

Figure 7 - Summary Tabulation of Accumulated Power in Spherical Modes for Two-Dipole Element

Figure 8 shows one polarization component of the element's far-field pattern. This pattern plot has been rotated to an equatorial orientation to avoid polarization effects. The *IsoFilter*<sup>TM</sup> sphere was then translated first along x, then y, to see how much of the element's power got

through the filter. The resulting rejection curves are plotted in Figure 9 and Figure 10 when the accumulated modal power levels for n= 1,2 & 3 are used as measures of the degree of rejection.

Notice that now the level of rejection for this x-polarized dipole element at 4λ separation is between 35 and 45 dB depending upon which value of the principal modal index is used.

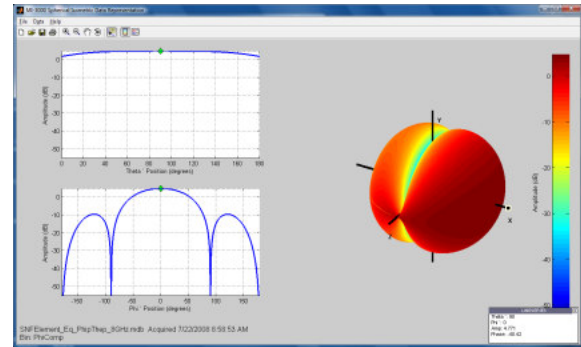


Figure 8 - Two-Dipole Element Pattern (φ Component)

For the cases of translation along the y- or z- axes, the rejection is significantly less, as shown by the plots in Figure 10.

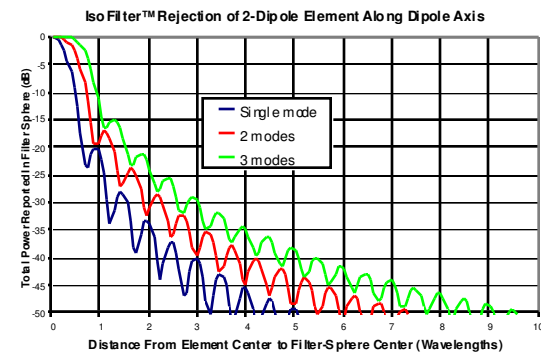


Figure 9 - Rejection Curve for Two-Dipole Element *IsoFilter*<sup>TM</sup> with Origin Translated Along x-Axis

### IV. APPLICATION OF ISOFILTER TO THE CASE OF A SIMULATED ARRAY OF SMALL ANTENNAS

To carry the simulation of *IsoFilter*<sup>TM</sup> over to the case of a set of antennas, we simulated a sparsely populated array of seven elements, where each element was again a two-dipole endfire radiator. A schematic of the array is shown in Figure 11 below. The array is sparsely populated to simulate a collection of antennas with several wavelengths of separation between each pair. There is a center element consisting of a single element and two sets of distant elements consisting of two elements and four elements respectively.

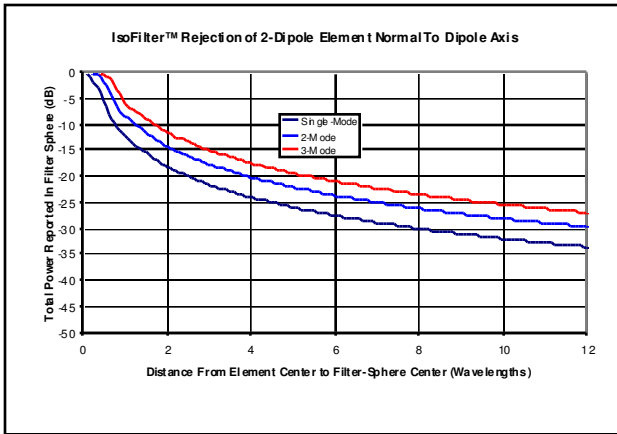


Figure 10 - Rejection Curve for Two-Dipole Element *IsoFilter™* with Origin Translated Along y-Axis or Along z-Axis

Each element position is separated from its nearest neighbor by 0.5 in. At a frequency of 11.8 GHz, this separation corresponds to half a wavelength; at lower frequencies, it is less than half a wavelength. Far-field patterns were computed for this sparse array at a variety of frequencies, causing the separation to vary in terms of wavelengths. No coupling among the elements was simulated, so the far field represents the summation of several offset isolated element patterns.

Each of the seven dipole pairs in this simulation is equally weighted. This means that of the three small antennas simulated, the one in the center that we are trying to isolate has the lowest level of excitation.

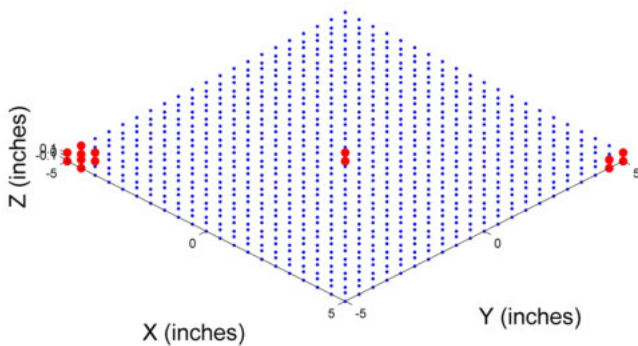


Figure 11 - Schematic of 21 X 21 Element Sparse Array

A sparse array such as this can be thought of as resembling a set of broad-beam antennas and/or scatterers on a vehicle, spacecraft, or other platform. The far field of this array exhibits rather dramatic interference among the elements. This is to be expected, since several wavelengths separate what are in effect three subarrays. The array's far-field pattern is shown in Figure 12 below. The result of *IsoFilter™* is exhibited by plotting the far-field pattern of the center single element after the *IsoFilter™* has been applied; Please see Figure 13.

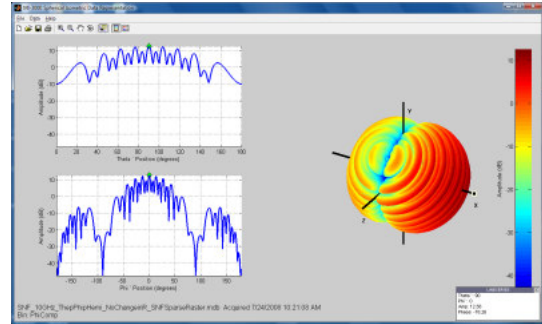


Figure 12 - Sparse Array's Far Field at 10.73 GHz.

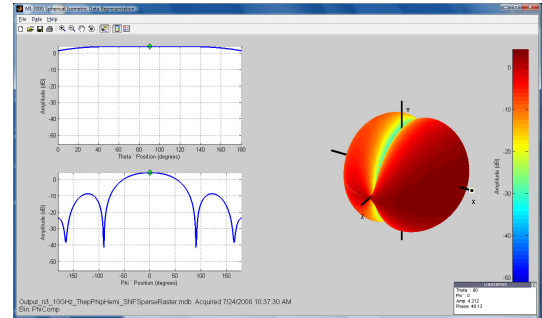


Figure 13 - Center Element of Array After *IsoFilter™*

An overlay of the two phi cuts, before and after *IsoFilter™* has been applied to the sparse array, is shown in Figure 14 below.

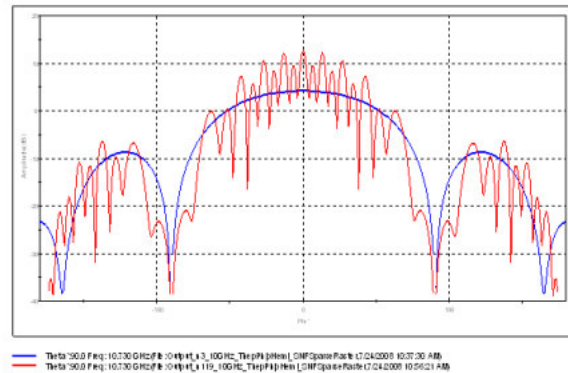


Figure 14 -Far Field of Sparse Array Before & After *IsoFilter™* to Center Element

The comparison shows that the *IsoFilter™* technique is very effective at removing the interference caused by the outer six elements. However, when one examines the comparison of the result of *IsoFilter™* to the true element pattern alone, he finds some residual discrepancy as evidenced by the comparison in Figure 15:

#### V. COMPARISON OF ISOFILTER™ TO IMAGING FOR THE SIMULATED ARRAY OF SMALL ANTENNAS

To complete our detailed investigation into the performance of *IsoFilter™*, we have used MI's conventional

aperture imaging software package to provide a benchmark for rejection.

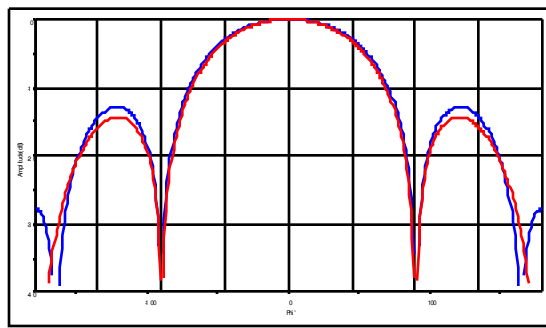


Figure 15 – Center-Element Far Field After *IsoFilter™* vs. Actual Far Field of Ideal Element

We take a high resolution image of a single center element available with the sparse array model corresponding to a frequency of 8.0 GHz. This is shown in Figure 11, which plots the top 30 dB of image levels over the 21 X 21 element array area - or a 10" by 10" region.

The visibly high sidelobe regions are distributed along the y-axis and the low sidelobe regions along the x-axis. A plot of the image level versus distance is shown in Figure 11, comparing the fall-off in the image along the x-axis, parallel to the dipole axis, and along the y-axis, normal to the dipole axis. We noted that conventional aperture imaging had significant difficulty interpolating the portion of the dipole pattern that gets divided by  $\cos(\theta)$ , which of course goes to zero at the boundary of real space. The  $\cos(\theta)$  term was artificially limited to 0.5 in order to get usable values in this analysis. This artificial tapering of the plane-wave spectrum may have reduced the side lobes shown in Figure 11.

For the comparison considered here, we focus first on the fall-off along the x-axis in the coordinate system of the single element.

Out of interest in making a comparison, we plot below in Figure 11, the rejection curve from the image of Figure 11 together with the *IsoFilter™* rejection curves of Figure 11. We find that the *IsoFilter™* technique when applied to separation of a source of radiation in a planar aperture has close-in resolution comparable to standard aperture imaging. However, the rejection levels at distances larger than a wavelength are better with aperture imaging. One should keep in mind that *IsoFilter™* would have several key advantages as a basis for diagnostic imaging: Firstly, one is free to locate the test points of the *IsoFilter™* origin arbitrarily, placing them anywhere within the volume of the original test sphere; whereas for aperture imaging one obtains the expected resolution only in the aperture plane.

Secondly, the *IsoFilter™* technique is intimately related to the pattern of the volume element being filtered; whereas with aperture imaging, the pattern of each pixel becomes lost in the digital processing.

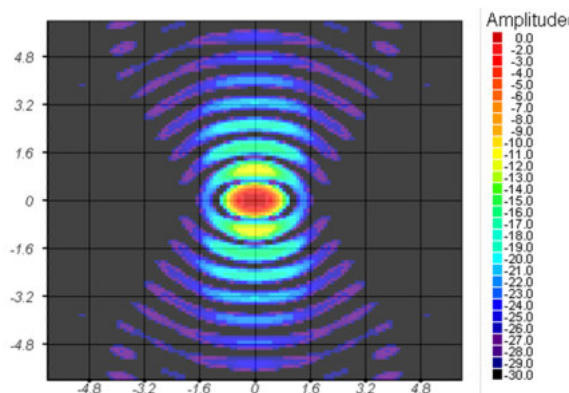


Figure 16 - Image of Single Element at 8 GHz

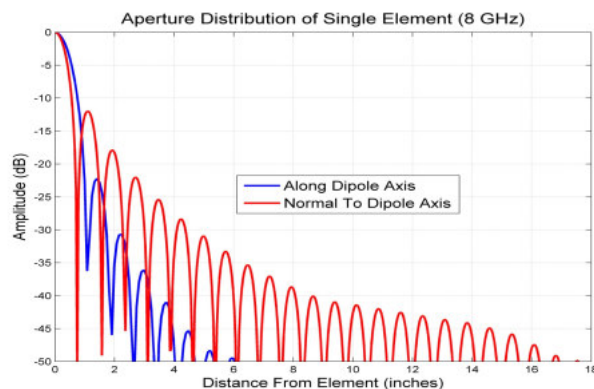


Figure 17 - Plot of Image Level vs. Distance for Single Element at 8.0 GHz

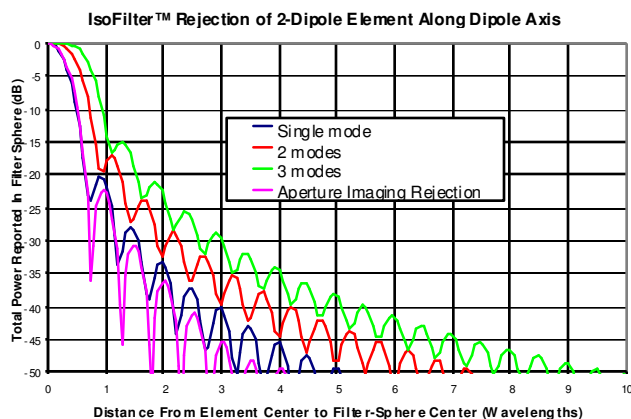


Figure 18 - Comparison - Plot of Image Level vs. Distance Along x-Axis for Single Element at 8.0 GHz Together with *IsoFilter™* Rejection Curves

#### REFERENCES

- [1] D.W.Hess and S. McBride, "Evaluation of *IsoFilter™* Fidelity in Selected Applications" AMTA 2008 Proceedings, Paper A08-0057, pp. 289-295, Boston, MA.